INTERNATIONAL JOURNAL OF HYDROGEN ENERGY 39 (2014) 3837–3854

Available online at www.sciencedirect.com

ScienceDirect

journal homepage: www.elsevier.com/locate/he

An improved TLBO with elite strategy for parameters identification of PEM fuel cell and solar cell models

Qun Niu [a,*], Hongyun Zhang [a], Kang Li [b]

[a] School of Mechatronic Engineering and Automation, Shanghai Key Laboratory of Power Station Automation Technology, Shanghai University, Shanghai 200072, China

[b] Energy, Power and Intelligent Control, School of Electronics, Electrical Engineering and Computer Science, Queen's University Belfast, Belfast BT9 5AH, UK

ARTICLE INFO

Article history:
Received 13 October 2013
Received in revised form
9 December 2013
Accepted 15 December 2013
Available online 1 February 2014

Keywords:
TLBO
Parameter identification
PEM fuel cell
Solar cell
Elite strategy

ABSTRACT

Clean and renewable energy generation and supply has drawn much attention worldwide in recent years, the proton exchange membrane (PEM) fuel cells and solar cells are among the most popular technologies. Accurately modeling the PEM fuel cells as well as solar cells is critical in their applications, and this involves the identification and optimization of model parameters. This is however challenging due to the highly nonlinear and complex nature of the models. In particular for PEM fuel cells, the model has to be optimized under different operation conditions, thus making the solution space extremely complex. In this paper, an improved and simplified teaching-learning based optimization algorithm (STLBO) is proposed to identify and optimize parameters for these two types of cell models. This is achieved by introducing an elite strategy to improve the quality of population and a local search is employed to further enhance the performance of the global best solution. To improve the diversity of the local search a chaotic map is also introduced. Compared with the basic TLBO, the structure of the proposed algorithm is much simplified and the searching ability is significantly enhanced. The performance of the proposed STLBO is firstly tested and verified on two low dimension decomposable problems and twelve large scale benchmark functions, then on the parameter identification of PEM fuel cell as well as solar cell models. Intensive experimental simulations show that the proposed STLBO exhibits excellent performance in terms of the accuracy and speed, in comparison with those reported in the literature.

1. Introduction

To tackle the twin challenges of secure and sustainable energy supply and sustainable environment, strict environmental laws and incentive energy policies have been introduced worldwide to encourage the development and utilization of alternative energy resources, such as wind, solar, fuel cell, wave, etc. Among various technologies, fuel cells and solar cells have drawn much attention for producing efficient and

* *Corresponding author*. Tel./fax: +86 021 56334241.
E-mail addresses: comelycc@hotmail.com, comelycc@gmail.com (Q. Niu).

0360-3199/$ – see front matter
http://dx.doi.org/10.1016/j.ijhydene.2013.12.110

clean electricity. Among the most popular fuel cells, polymer electrolyte membrane (PEM) fuel cell has many favorable characteristics, including relatively low operating temperatures, superior durability, high power density, low noise and zero emission. Likewise, as one of the fastest growing renewable power generation technologies, solar cell is not only capable of directly converting solar energy to electricity, but also has promising features like easy installation, little maintenance, no pollution and noise-free.

A key issue for effective and efficient utilizations of the PEM fuel cells and solar cells is the optimal modeling, and models have been developed to represent the behavior of the system at different operating conditions. It is well known that mathematical models of these cells are usually composed of a set of unknown parameters and exhibit non-convex and highly nonlinear nature. Further, PEM fuel cell and solar cell models are multivariate, strongly coupled, and model parameters vary with operation conditions. Therefore, it is vital to produce more accurate models that can better reveal the actual behavior of PEM fuel cells and solar cells, in particular, the precise identification of unknown parameters in these models. This is particularly important for PEM fuel cells where the model has to be optimized under different operation conditions with different data sets, thus making the solution space extremely complex. The key to the problem is the proposal of effective optimization methods for the identification of the model parameters.

Generally, traditional analytic methods such as gradient method, lambda iteration method, conjugate direction method, and linear programming are popular for optimization problems due to their deterministic nature and computational efficiency for small-scale problems. However, these methods also have their limitations. For instance, convex objective function is needed for gradient method. Linear programming requires the linearity of the objective function and large errors may be generated for problems with nonlinear features. Further, many traditional methods are highly sensitive to the initial values and often converge to local optimums. These limitations restrict the application of traditional methods to the parameter identification of PEM fuel cell and solar cell models which are highly nonlinear and strongly coupled, and the optimization exhibits non-convex characteristics. In particular, for PEM fuel cells, the model has to be optimized under different operation conditions using different data sets, which makes the solution space extremely complex.

As a kind of stochastic methods inspired by natural phenomenons, meta-heuristic methods have proved to a promising alternative to tradition approaches. They impose no restrictions on the problem formulation, and can be easily adapted for various real world problems. In the past decade, a number of meta-heuristic methods have been proposed and successfully applied to solve various optimization problems, such as vehicle routing planning, mechanical engineering design, signal processing, chemical engineering, machine intelligence and pattern recognition. They have also been applied to the parameters identification of PEM fuel cell and solar cell models. For example, a niche hybrid genetic algorithm (HGA) was proposed to identify the model parameters of PEM fuel cell under four different operating conditions [1]. Subsequently, several GA variants were developed to further improve the accuracy and performance of the model, such as real coded GA (Real GA) [2] and adaptive RNA genetic algorithm (ARNA-GA) [3]. Besides, several other methods were used to solve the problem, including differential evolution (DE) [4], a novel P systems based method (BIPOA) [5], particle swarm optimization (PSO) [6], a grouping-based global harmony search algorithm (GGHS) [7], an innovative global harmony search algorithm (IGHS) [8] and a new heuristic method called bird mating optimizer [9]. The parameter identification of solar cell models have also been addressed by chaos PSO (CPSO) [10], simulated annealing (SA) [11], pattern search (PS) [12], artificial bee swarm optimization (ABSO) algorithm [13] and an improved adaptive differential evolution algorithm (IADE) [14]. A new nature-inspired algorithm that is proposed recently, namely the bird mating optimizer (BMO) [15] has also been used for the parameter estimation of fuel cell polarization curve. Despite a number of progresses have been made to improve the searching capability, stability and scalability of the meta-heuristic approaches for different problems are still the major issues for the successful application of these methods to practical real-life problems. For example, it is time consuming to set effective parameters for SA and BIPOA. PSO, GA and their variants may suffer from premature convergence. Further, none of these aforementioned methods have been successfully used to solve the model parameter identification problems for these two type of cells due to the scalability issue of these methods. Therefore, it is vital to develop effective and simplified meta-heuristic methods which have fewer parameters to set and have the scalability for both the PEM fuel cell and solar cell modeling problems.

Teaching-learning-based optimization (TLBO) is a new meta-heuristic method proposed by Rao et al. for constrained mechanical design optimization problems [16]. It has fewer adjustable parameters and requires no other parameters except two commonly used parameters, namely the population size and the number of generation or iteration, which are the two basic ones for population based evolutionary algorithms. Different from TLBO, many methods like GA, DE and PSO, need a few more design parameters to improve the performance. For instance, crossover and mutation probabilities (P_c and P_m) are two additional key parameters for GA, DE requires choosing a suitable scalar number F and crossover probability (P_c), and PSO needs careful selection of the acceleration parameters and the ranges of flying velocities. All these additional parameters need to be carefully tuned for each specific problem and inevitably will significantly increase the difficulties for the users to balance the choices of values for these parameters in order to achieve good results for a specific optimization problem. Hence, a method with fewer parameters like TLBO is a good choice for users in solving many real world engineering optimization problems.

Recently, the elite individual is used to replace the worst solution in TLBO to improve the exploration and exploitation capabilities, and the proposed method was employed to optimize the constrained problems [17]. Additionally, its performance was also confirmed on a series of unconstrained benchmark problems [18]. However, compared with other population based method, the TLBO also has its drawbacks. As pointed by Crepinsek [19], the population is evaluated twice in

one generation in the original TLBO, which may cause the TLBO unable to make the best performance within a limited number of function evaluations. Therefore, it is meaningful to further improve the TLBO performance and reduce the evaluation cost in one generation or iteration.

In this paper, an improved and simplified TLBO with elite strategy, namely STLBO is proposed to improve the quality of solutions and applied to the parameter identification of PEM fuel cell and solar cell models. In the proposed STLBO, an elite strategy is employed to improve the searching capability, and a chaotic map is used to enrich the uniformity of random values in mutation phase. Similar to the basic TLBO, STLBO retains the advantages of simplicity in concept and easy implementation. But compared with the basic TLBO, the structure of the proposed method is further simplified, and the function evaluation number in one generation is significantly reduced. To evaluate the performance of STLBO, it is tested on two low dimensions decomposable problems and twelve large scale benchmark functions, and compared with the basic TLBO and six commonly used methods, including SaDE, GL-25, PSO-IW, PSO-CF, IHS and GA. Comparison results show the effectiveness of the proposed method. Then, STLBO is employed to identify the parameters for both PEM fuel cell and solar cell models, and the comparison with the reported results in the literature demonstrates the effectiveness and scalability of the proposed STLBO in solving complicated real world problems.

The rest of this paper is organized as follows. Section 2 is the problem formulation for PEM fuel cell and solar cell modeling. Basic TLBO algorithm is introduced in Section 3. The proposed STLBO and its implementation are detailed in Section 4. In Section 5, the proposed method is tested on a group of benchmark problems and compared with several commonly used meta-heuristic methods. In Section 6, STLBO is employed to solve the PEM fuel cell and solar cell modeling problems. Finally, some remarks and conclusions are given in Section 7.

2. Problem formulation

In this section, the proton exchange membrane (PEM) fuel cell model as well as the solar cell model are introduced.

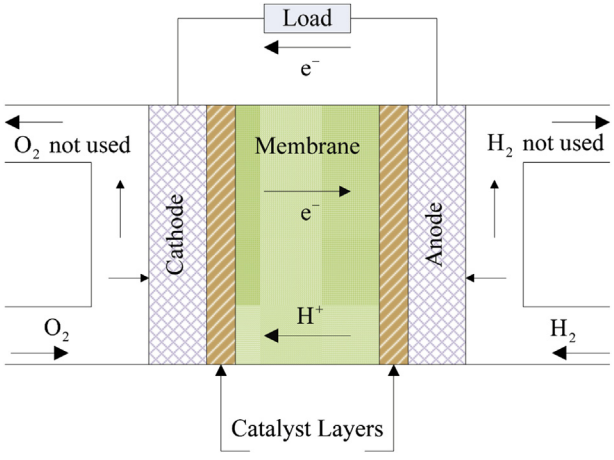

Fig. 1 – Simple scheme of a single PEM fuel cell.

2.1. PEM fuel cell model

2.1.1. Operation principle of PEM fuel cell

PEM fuel cell is a device that can convert chemical energy into electrical energy directly by electrochemical process. Similar to a battery, it is generally composed of a cathode and an anode electrode, which are separated by a polymer electrolyte membrane. Fig. 1 illustrates the basic scheme for a single PEM fuel cell. In normal operation of a PEM fuel cell, the hydrogen is fed continuously to the anode, and the oxidant, oxygen or air, is fed continuously to the cathode. The hydrogen (H_2) and oxygen (O_2) have a strong chemical affinity, and the chemical reactions of the PEM fuel cell are formulated as follows:

Oxidation reaction in the anode : $2H_2 \rightarrow 4H^+ + 4e^-$

Reduction reaction in the cathode : $4H^+ + 4e^- + O_2 \rightarrow 2H_2O$

Overall reaction : $2H_2 + O_2 \rightarrow 2H_2O$

During electrical reactions and electron transfer process, an electromotive force is generated between the two electrodes. Many single cells can be assembled into a fuel cell stack in order to meet the required amount of power. Importantly, the PEM fuel cell needs a quite low operating temperature, which typically ranges from 70 to 85 °C, and is very safe in applications.

2.1.2. PEM fuel cell stack modeling

The fuel cell model proposed in Ref. [20] is considered in this paper and the electrical equivalent circuit of a single PEM fuel cell is represented in Fig. 2. R_{act} is activation equivalent resistance, R_{con} is the concentration equivalent resistance, and the equivalent capacitance C can smooth the voltage drop across R_{act} and R_{con} effectively. The output voltage of a single fuel cell can be defined as [21]

$$U_{cell} = E_{Nernst} - U_{act} - U_{\Omega} - U_{con} \quad (1)$$

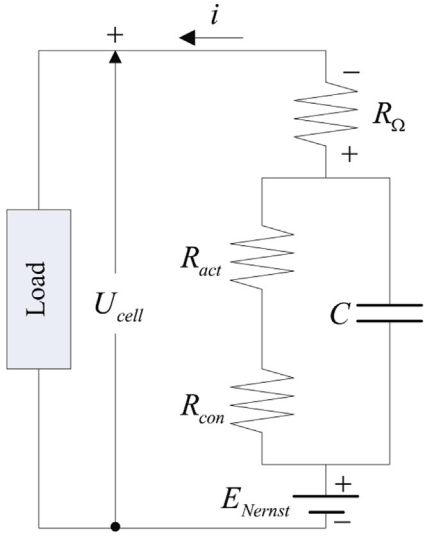

Fig. 2 – Equivalent electrical circuit of a single PEM fuel cell.

where U_{cell} (V) is the fuel cell output voltage at a certain operating condition, E_{Nernst} (V) is the reversible voltage; U_{act} (V) is the voltage drop due to the activation of the anode and cathode; and U_{Ω} and U_{con} (V) are the ohmic and concentration voltage drops, respectively.

In order to generate required amount of power, a number of single fuel cell can be assembled into a fuel cell stack system. For a stack with n cells, the voltage can be calculated by Ref. [20,21]

$$U_s = n \times U_{cell} \tag{2}$$

where U_s is the stack voltage and n is the number of series connected cells in the stack.

(a) Reversible voltage E_{Nernst}

The reversible voltage is produced by a cell without any irreversibility. A form of the Nernst equation is used since it allows to investigate the performance in view of temperature, system pressure, and the particle pressure of both hydrogen and oxygen. It can be obtained by Ref. [22].

$$E_{Nernst} = 1.229 - 0.85 \times 10^{-3}(T - 298.15) + 4.3085 \times 10^{-5} T \times \left(\ln(P_{H_2}) + 0.5 \ln(P_{O_2})\right) \tag{3}$$

where variable T (K) denotes the cell operation temperature; P_{H_2} and P_{O_2} are the effective partial pressure (atm) of hydrogen and oxygen, respectively. Suppose the reactants are H_2 and O_2, then the partial pressures can be calculated as follows

$$P_{O_2} = RH_c \cdot P_{H_2O} \cdot \left[\left(\exp\left(\frac{4.192 \cdot (i/A)}{T^{1.334}} \right) \times \frac{RH_c \cdot P_{H_2O}}{P_c} \right)^{-1} - 1 \right] \tag{4}$$

$$P_{H_2} = 0.5 \cdot RH_a \cdot P_{H_2O} \cdot \left[\left(\exp\left(\frac{1.635 \cdot (i/A)}{T^{1.334}} \right) \times \frac{RH_a \cdot P_{H_2O}}{P_a} \right)^{-1} - 1 \right] \tag{5}$$

where RH_a and RH_c are the relative humidity of vapor in the anode and cathode; P_a and P_c are the anode and cathode inlet pressure (atm); i (A) is the cell operating current; A is the activation area of the membrane, and P_{H_2O} represents the saturation pressure of the water vapor (atm), which can be expressed as a function of the cell temperature T [1,23].

$$\log(P_{H_2O}) = 2.95 \times 0.01 \times (T - 273.15) - 9.18 \times 10^{-5} \times (T - 273.15)^2 + 1.44 \times 10^{-7} \times (T - 273.15)^3 - 2.18 \tag{6}$$

(b) Activation voltage drop U_{act}

U_{act}, which is caused by the sluggish kinetics of the reactions taking place on the active surface of electrodes, can be expressed as follows [22].

$$U_{act} = -\left[\xi_1 + \xi_2 \times T + \xi_3 \times T \times \ln(C_{O_2}) + \xi_4 \times \ln(i)\right] \tag{7}$$

where ξ_1, ξ_2, ξ_3 and ξ_4 are parametric coefficients for each cell model, whose values are defined based on theoretical equations with kinetic, thermodynamic and electrochemical foundations; C_{O_2} is the concentration of dissolved oxygen (mol/cm^3) on the interface of the cathode catalyst, which can be calculated by Henry's law expression as follows

$$C_{O_2} = \frac{P_{O_2}}{5.08 \times 10^6 \times e^{-(498/T)}} \tag{8}$$

(c) Ohmic voltage drop U_{Ω}

The ohmic voltage drop is caused by the voltage drop through the equivalent membrane resistance R_M, and contact resistance R_C both between the membrane and electrodes, as well as the electrodes and the bipolar plates. It can be obtained by using the Ohm's law as follows

$$U_{\Omega} = i \times (R_M + R_C) \tag{9}$$

Further, according to Ohm's law, the equivalent resistance of the membrane R_M can be calculated as

$$R_M = \frac{\rho_M \cdot l}{A} \tag{10}$$

where l is the thickness of the membrane (cm), which serves as the cell's electrolyte; ρ_M is the specific resistively of the membrane for the electron flow (Ω cm), which can be obtained by the following numeric expression [22].

$$\rho_M = \frac{181.6 \cdot \left[1 + 0.03 \cdot (i/A) + 0.062 \cdot (T/303)^2 \cdot (i/A)^{2.5}\right]}{[\lambda - 0.634 - 3 \cdot (i/A)] \cdot \exp[4.18 \cdot (T - 303)/T]} \tag{11}$$

where λ is the water content of the membrane, which is an adjustable parameter from a possible maximum value.

(d) Concentration voltage drop U_{con}

Concentration voltage drop is caused by the mass transportation, which affects the concentrations of hydrogen and oxygen. It can be determined by

$$U_{con} = -b \cdot \ln\left(1 - \frac{J}{J_{max}}\right) \tag{12}$$

where b is a parametric coefficient (V) that depends on the cell and its operation condition. J is the actual cell current density (A/cm^2), and J_{max} is the maximum value of J.

$$J = i/A \tag{13}$$

With above formulations, the PEM fuel cell stack model can be built up easily. As long as the seven unknown parameters (ξ_1, ξ_2, ξ_3, ξ_4, λ, b, R_C) are determined, the output U_s corresponding to a certain input i can be predicted immediately.

2.1.3. *Objective function*

A desirable PEM fuel cell stack model should match the actual output characteristic as closely as possible. In this paper, sum of the squared error (SSE) between the voltage of the PEM fuel cell stack model and experimental measured voltage of the actual PEM fuel cell stack is used as the objective function for optimization to determine seven unknown model parameters [1]

$$\text{miny} = \sum_{j=1}^{S} \sum_{k=1}^{N} \left(U_{sm,jk} - U_{s,jk}\right)^2 \tag{14}$$

where y is the objective function, $U_{sm,jk}$ is the experimental data of PEM fuel cell stack voltage, $U_{s,jk}$ is the model output voltage obtained by Eq. (2), S is the number of data set for identification, N is the number of data in each data set.

2.2. Solar cell model

The parameters estimation of solar cell model focuses on minimizing the differences between the measured and simulated solar cell current at various environmental conditions. It is essential to have an accurate mathematical solar cell model before proceeding to the estimation phase. Despite the fact that numerous equivalent circuit models have been developed and proposed to describe the $I-U$ characteristic of solar cells, while only two models are commonly used in practice, including the double diode model and single diode model. In this section, these two models are presented briefly.

2.2.1. Double diode model

The solar cell is commonly modeled as a current source connected in parallel with a rectifying diode. However, in practice the current source is also shunted by another diode that models the space charge recombination current and shunt leakage resistor to account for the partial short circuit current path near the cell's edges due to the semiconductor impurities and non-idealities. Further, a resistor is connected in series with the cell shunt elements due to the solar cell metal contacts and the semiconductor material bulk resistance [24]. The equivalent circuit for this model is illustrated in Fig. 3, which shall become the basis for parameter estimation in this paper.

The solar cell terminal current of the double diode model is obtained as follows,

$$I = I_{ph} - I_{d1} - I_{d2} - I_{sh} \tag{15}$$

where I denotes the terminal current (A); I_{ph} represents the total current generated by the solar cell for a given lighting and temperature conditions (A); I_{d1} and I_{d2} are the first and second diode current, respectively (A); and I_{sh} denotes the shunt resistor current (A).

According to the Shockley equation, the terminal current I can be formulated as follows,

$$I = I_{ph} - I_{sd1}\cdot\left[\exp\left(\frac{q\cdot(U_t + R_s\cdot I)}{n_1\cdot k\cdot T_0}\right) - 1\right] - I_{sd2}\cdot\left[\exp\left(\frac{q\cdot(U_t + R_s\cdot I)}{n_2\cdot k\cdot T_0}\right) - 1\right] - \frac{U_t + R_s\cdot I}{R_{sh}} \tag{16}$$

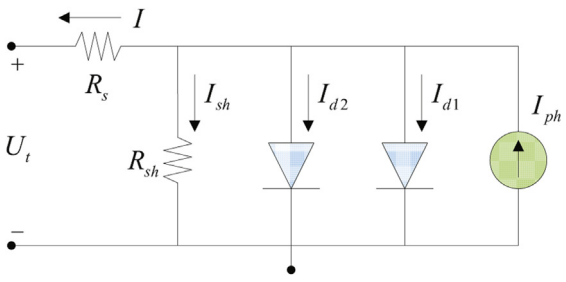

Fig. 3 – Equivalent circuit of a double diode solar cell model.

where R_s and R_{sh} are the series and shunt resistances, respectively (Ω); U_t is the terminal voltage (V); I_{sd1} and I_{sd2} are the diffusion and saturation currents respectively; n_1 and n_2 represent the diffusion and recombination diode ideality factors; q is the electronic charge (1.60217646E-19 C); k is the Boltzmann's constant (1.3806503E-23 J/K); and T_0 is the cell absolute temperature in Kelvin (K).

For this double diode solar cell model, there are seven parameters to be estimated, including R_s, R_{sh}, I_{sd1}, I_{sd2}, n_1, n_2 and I_{ph}, which are very important to reflect the solar cell performance as well as that of an actual system.

2.2.2. Single diode model

Single diode model has been used to represent the static characteristic of solar cell widely, and it has been employed successfully to fit measured data. This model is developed by combining both diode currents together with the introduction of a non-physical diode ideality factor n. The equivalent circuit of this model is shown in Fig. 4, and the terminal current I of this model is reduced to the following equation

$$I = I_{ph} - I_{sd}\cdot\left[\exp\left(\frac{q\cdot(U_t + R_s\cdot I)}{n\cdot k\cdot T_0}\right) - 1\right] - \frac{U_t + R_s\cdot I}{R_{sh}} \tag{17}$$

In this model, the parameter estimation problem reduces to find five parameters, including R_s, R_{sh}, I_{sd}, I_{ph} and n.

2.2.3. Objective function

The performance of the estimated parameters is evaluated by an objective function Y, which is formulated as the root mean square of the difference between the simulated and measured current data. For an $I-U$ data set with N current values, Y can be defined as follows,

$$\min Y = \sqrt{\frac{1}{N}\sum_{i=1}^{N}\left(I_i - I_{m,i}\right)^2} \tag{18}$$

where N is the number of measured data; I_i and $I_{m,i}$ are the i^{th} simulated and measured current value, respectively.

I_i can be obtained by Eqs. (19) and (20) for double diode mode and single diode model, which can be rewritten as

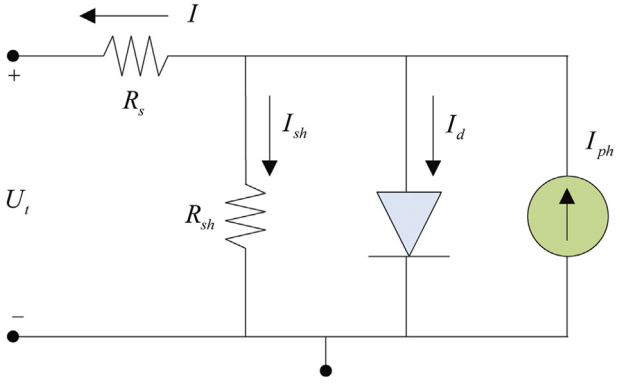

Fig. 4 – Equivalent circuit of a single diode solar cell model.

$$I_i = I_{ph} - I_{sd1}\cdot\left[\exp\left(\frac{q\cdot(U_{t,i}+R_s\cdot I_{m,i})}{n_1\cdot k\cdot T_0}\right)-1\right] - I_{sd2}\cdot\left[\exp\left(\frac{q\cdot(U_{t,i}+R_s\cdot I_{m,i})}{n_2\cdot k\cdot T_0}\right)-1\right] - \frac{U_{t,i}+R_s\cdot I_{m,i}}{R_{sh}} \quad (19)$$

$$I_i = I_{ph} - I_{sd}\cdot\left[\exp\left(\frac{q\cdot(U_{t,i}+R_s\cdot I_{m,i})}{n\cdot k\cdot T_0}\right)-1\right] - \frac{U_{t,i}+R_s\cdot I_{m,i}}{R_{sh}} \quad (20)$$

where $U_{t,i}$ denotes the i^{th} measured voltage value.

The objective of parameters estimation for solar cell model is to minimize Y with respect to Φ, where $\Phi = [R_s, R_{sh}, I_{ph}, I_{sd1}, I_{sd2}, n_1, n_2]$ in the double diode model, and $\Phi = [R_s, R_{sh}, I_{ph}, I_{sd}, n]$ in the single diode model.

3. Overview of basic TLBO algorithm

In this section, the basic concept of TLBO is presented briefly.

TLBO is a new population based meta-heuristic method proposed by Rao et al. [16], which was inspired by the interaction of the teacher and learners. This method has two key components, namely the teacher and learners. The teacher is generally considered as the most knowledgeable person in a class who shares his/her knowledge to improve the grade/performance of the whole class. Trained by a high-quality teacher, learners can achieve better result quickly. Further, learners can also learn through the interaction and communication among themselves, which can also help to improve their performance. The whole operating process of TLBO can be summarized in two phases: the teacher phase and the learner phase. The "Teacher phase" means learning from the teacher, and the "Learner phase" means learning through the interaction among learners.

3.1. Teacher phase

In the teacher phase, the teacher tries to improve the mean performance of the class by his/her own capability. However, the improvements of each learner are dependant on their own learning capabilities. The teacher phase can be formulated as follows,

$$P_{new,i} = P_i + r_1\cdot[\text{teacher} - T_F\cdot\text{Mean}] \quad (21)$$

where $P_{new,i}$ is a newly generated individual according to P_i; r_1 is random real value in the range of 0 and 1; teacher represents the global best individual in current population; T_F denotes the teaching factor, which can be either 1 or 2 and determined randomly with the same probability, and Mean is the mean of the current population. The newly generated $P_{new,i}$ will be accepted if and only if it performs better than the old individual P_i.

3.2. Learner phase

In this phase, the learners enhance their performance by interaction among themselves. A learner interacts with other two randomly selected individuals to further improve his/her performance. The learner phase can be expressed below,

For $i = 1$ to ps
  Randomly select other two learners P_m and P_n, $(m \neq n \neq i)$
  if P_m is better than P_n
    $P_{new,i} = P_i + r_i\cdot(P_m - P_n)$
  else
    $P_{new,i} = P_i + r_i\cdot(P_n - P_m)$
  end
End

where ps denotes the population size; r_i is a random real value in the range of 0 and 1. $P_{new,i}$ will be accepted if it is better than P_i.

4. The proposed method and its implementation

4.1. The simplified TLBO with elite strategy

Since the introduction of TLBO, it has been applied in various optimization problems, such as heat exchangers [25], reserve constrained dynamic economic dispatch problem [26], optimal distribution generation location and size [27], and parameter optimization of modern machining process [28]. Reported results show that TLBO has good exploration capability and can find potential optimum rapidly. Moreover, compared with other evolutionary algorithms, such as ES, DE, PSO, GA and ABC, TLBO has very few parameters, which is very convenient for implementation. As it was pointed out in Ref. [19], a major drawback of the basic TLBO is that many more function evaluations are consumed in each generation/iteration in comparison with other population based methods, which may lead to a poor convergence rate for the basic TLBO within a limited number of function evaluations. Although all learners are expected to be improved via learning from the global best teacher, the results may be affected significantly by the randomness of teaching factor (T_F). Further, little attention has been paid to improve the global best, which also leads to slow convergence.

To improve the searching capability of the basic TLBO within a limited FES, a simplified TLBO with elite strategy (STLBO) is developed in this paper. Compared with the basic TLBO, the major advantages of the proposed STLBO are simple in concept, lower FES cost and easier to implement. Like the basic TLBO, there is no need to manually tune any parameters in STLBO except the population size. In the proposed STLBO, the teacher phase is redefined and simplified, while the learner phase remains unchanged. In the redefined reacher phase, a local search operation is used to further improve the current global best, and an elite strategy is introduced to update the current worst learner. The redefined teacher phase can be expressed as follows

$$\text{New}(1,k) = \begin{cases} \text{teacher}(1,k) + mu, & \text{if rand} < \mu \\ \text{teacher}(1,k), & \text{else} \end{cases} \quad (22)$$

where New is a new solution found around the current best teacher, k denotes the k^{th} decision variable in a solution, and $k \in \{1, 2, \ldots, \text{Dim}\}$; mu is a random mutation variable used in the local search operation; rand is a uniformly distributed real value in the range of [0,1]; μ is the mutation probability.

Through the mutation variable, the local search attempts to find better solution around the current best teacher. If the new solution is better than the worst one, the elite strategy will be used to replace the worst learner with the new solution, which can be formulated as follows,

$$\mathrm{Wst} = \begin{cases} \mathrm{New}, & \text{if } f(\mathrm{New}) < f(\mathrm{Wst}) \\ \mathrm{Wst}, & \text{else} \end{cases} \tag{23}$$

where Wst represents the worst one in current population, $f(\cdot)$ means the objective function value of corresponding solution.

During this phase, only one function evaluation is needed, which reduces the FES cost significantly.

To make the local search perform effectively, the mutation probability for each decision variable in teacher decreases linearly with the increase of FES, which can be formulated as follows,

$$\mu = 1 - FES/\mathrm{Max\_FES} \tag{24}$$

At the early stage, a larger μ helps to search in a larger solution and approach the optimum quickly. While during the latter optimization process, as the teacher is quite close to the global optimum, and mutation with a smaller probability acts as a fine searching mechanism to enhance the local searching capability, which is an effective strategy.

As the mutation is utilized for local searching, the magnitude of the mutation should not be large, otherwise it will make the new solution get further away from the current best and fail to reach a better one. In view of this, the magnitude of mutation is always limited to [−1,1] throughout. Generating random sequence with good uniformity is very important for the performance of mutation operation. In order to enrich the mutation behavior, the chaotic sequence is introduced to generate value for the mutation parameters. Chaotic sequence is a deterministic random-like process found in non-linear dynamic systems, which is non-periodic, non-converging and bounded. One of the simplest chaotic maps, logistic map was proposed in Ref. [29]. It exhibits chaotic dynamics when the control parameter is set to 4 and initial value $X_0 \notin \{0, 0.25, 0.5, 0.75, 1\}$. The process of this chaotic map is defined as follows

$$X_{n+1} = 4.0 \times X_n \times (1 - X_n) \tag{25}$$

where n is the iteration number, and X_n is the value of n^{th} chaotic iteration.

Thus, the mutation variable *mu* can be calculated as follows,

$$mu = 2 \times X_n - 1 \tag{26}$$

where the initial value X_0 is randomly selected from [0,1].

Formulation of New can be rewritten as follows, and detailed information of the proposed STLBO is illustrated in Fig. 5.

$$New(1,k) = \begin{cases} \mathrm{teacher}(1,k) + 2 \times X_n - 1, & \text{if rand} < \mu \\ \mathrm{teacher}(1,k), & \text{else} \end{cases} \tag{27}$$

4.2. *Implementation of STLBO for numerical optimization*

In this section, the proposed STLBO procedure for solving numerical optimization problems is presented in detail.

Input: *ps*: the size of the population; *LB*: lower boundary; *UB*: upper boundary; *Dim*: the number of decision variables; *Max_FES*: maximum number of function evaluations
/* **Initialization**:*/
FES = 0
For *i* = 1 to *ps*
for *k* = 1 to *Dim*
P(*i*,*k*) = *rand*×[UB_k-LB_k]+LB_k
end for
End For
Evaluate the objective function values of *P*
FES = *FES* + *ps*
X = *rand* / *initialization of chaos map* /
/* **Main loop**:*/
while *FES* < *Max_FES*
// **Redefined and simplified teacher phase** //
X = 4.0×*X*×(1-*X*) / *update the chaos map value* /
For k = 1to Dim
if *rand* < 1 – *FES*/*Max_FES*
New(1,*k*) = *teacher*(1,*k*) + (2×*X*-1)
end if
End For
Evaluate the objective value of new individual *New*
FES = *FES* + 1
if *New* is better than *Wst* / *Wst means the worst one in P* /
Wst = *New*
end if
// **Learner phase** //
For *i* = 1 to *ps*
Select other two learners randomly: $m \neq n \neq i$
if learner *m* is better than *n*
$P_{new,i} = P_i + rand(1,Dim).\times[P_m - P_n]$
else
$P_{new,i} = P_i + rand(1,Dim).\times[P_n - P_m]$
end if
end For
Evaluate the objective function values of P_{new}
FES = *FES* + *ps*
Update *P*: if the new is better than old in *P*, accepted it and replace the old one
End while
Output: the individual with the smallest objective function value in the population

Fig. 5 – Pseudo code of proposed STLBO.

Step 1. Input data

Set value for *ps*,*LB*,*UB*,Dim and Max_*FES*

Step 2. Initialization

Set $FES = 0$, and all solutions in the initial population *P* are generated randomly from their corresponding search space [*LB*,*UB*], which can be obtained as follows

$$P_{i,k} = \mathrm{rand} \times (UB_k - LB_k) + LB_k \tag{28}$$

Step 3. Objective function evaluation

The objective function is calculated for each individual in population *P*, and update $FES = FES + ps$.

Step 4. Redefine teacher phase

Firstly, generate a new solution New using local search;

Secondly, boundary constraints handling for the new generated individual New, which is operated as below

$$New(1,k) = \begin{cases} \mathrm{New}(1,k), & \text{if } LB_k \le New(1,k) \le UB_k \\ LB_k, & \text{if New}(1,k) < LB_k \\ UB_k, & \text{if New}(1,k) > UB_k \end{cases} \tag{29}$$

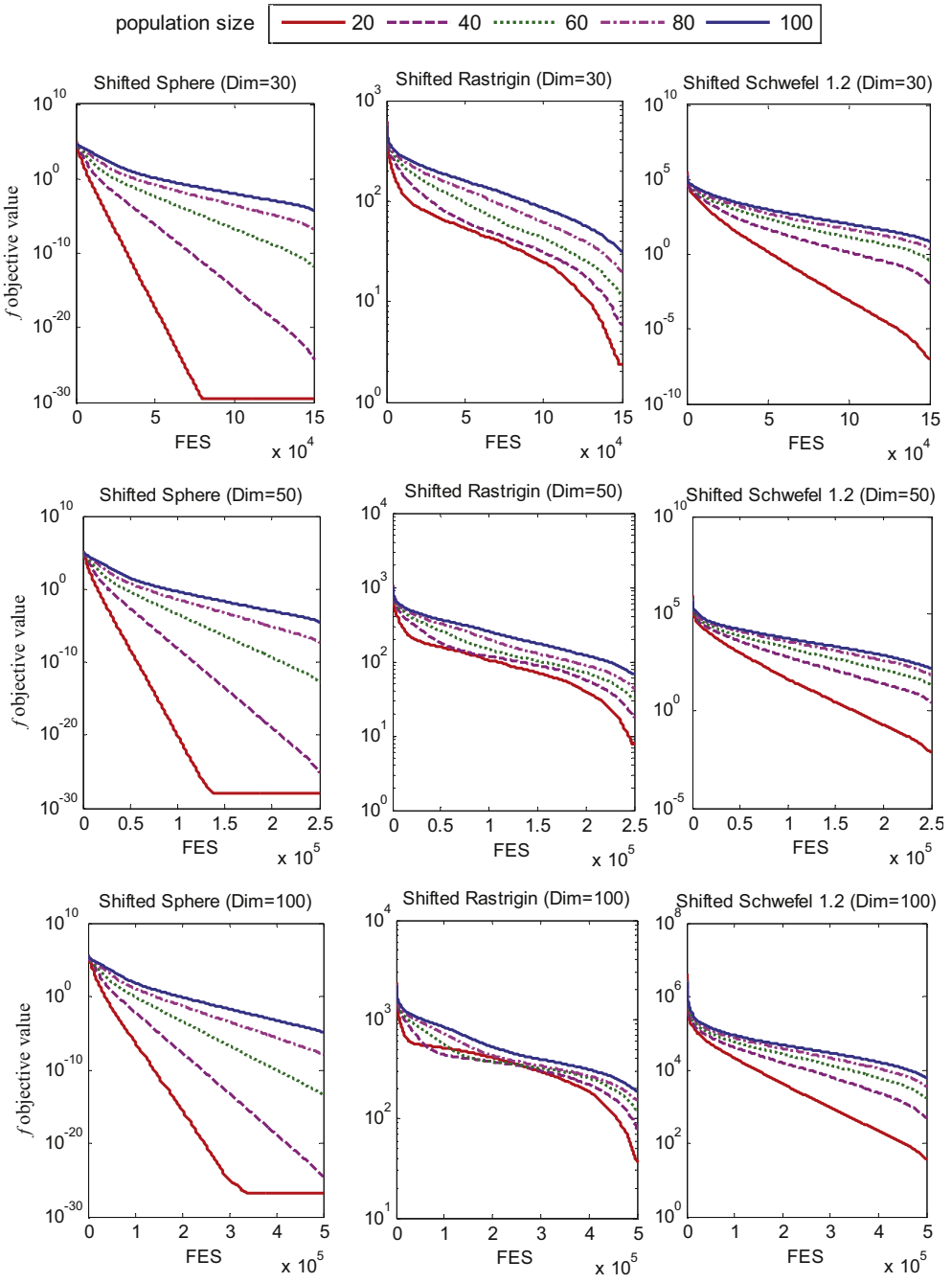

Fig. 6 – Mean convergence characteristics of STLBO with different population size.

Thirdly, calculate the objective function value of New and update $FES = FES + 1$. If it is better than Wst, the Wst will be replaced by New.

Step 5. Learner phase

Firstly, a new population P_{new} is produced according to the pseudo codes given in Fig. 5;

Secondly, boundary constraints handling for the new produced P_{new}, which is same with that in the refined teacher phase;

Thirdly, the objective function of P_{new} will be evaluated, and update $FES = FES + ps$;

Finally, update the population according to the greedy selection strategy, which is given below

$$P_i = \begin{cases} P_i, & \text{if } f(P_i) \le f(P_{new,i}) \\ P_{new,i}, & \text{if } f(P_i) > f(P_{new,i}) \end{cases} \tag{30}$$

Step 6. Termination criterion

Stop and output the best solution if the Max_*FES* is reached; otherwise go to *Step* 4.

5. Evaluation of STLBO on benchmark optimization problems

In this section, two real-valued decomposable problems with low dimensions [30] and 12 commonly used large scale benchmark functions with different characteristics taken from Refs. [31–33] are used to assess the scalability of the proposed method in comparison with the basic TLBO [34] and other six commonly used methods in the literature, namely SaDE [35], GL-25 [36], IHS [37], PSO-CF [38], PSO-IW [39] and GA-Toolbox (GA-TB). The GA-TB used for comparison was developed by the Department of Automatic Control and Systems Engineering of the University of Sheffield, which is available at http://www.acse.dept.shef.ac.uk/cgi-bin/gatbx-download. All simulation experiments were carried out using Matlab 7.0 and programmes were executed on an Intel(R) Core (TM) i3-2100 CPU 3.10 GHz personal computer.

5.1. *Parameter tuning*

Parameter setting has significant impact on the performance of heuristic methods. In STLBO, the population size is the only one parameter that needs to be tuned. To make the proposed STLBO achieve relative better results on problems with different characteristics, a comprehensive evaluation of the population size was carried out on three commonly used benchmark functions, including Shifted Sphere, Shifted Rastrigin and Shifted Schwefel 1.2. Sphere and Schwefel 1.2 are unimodal functions, while Rastrigin is a multimodal one. Details about the three problems are described in section 5.3. Further, the effectiveness of the linearly decreasing strategy on mutation probability proposed in this paper is also investigated in comparisons with other two constant values.

5.1.1. *Effect of population size*

In order to make a comprehensive evaluation on the effect of the population size, the STLBO was tested on the three problems with dimensions of 30, 50 and 100, respectively. 50 independent trials were carried out on each of these cases. Fig. 6 illustrates the convergence performance of STLBO with different population size in terms of the mean results over 50 runs. It is shown that STLBO with population size 20 achieved the best results on all three test problems with dimensions of 30, 50 and 100, respectively. The performance of STLBO degrades gradually as the population size increases, especially for function Shifted Sphere. Larger population size may unnecessarily increase the number of function evaluations, which leads to poor final results. From Fig. 6, we can also see that the population size affects the convergence speed. When population size is set to 20, a faster convergence velocity can be obtained. In view of these results, we can conclude that when population size is 20, the STLBO has shown an excellent searching ability and scalability for all these test problems. Hence, the population size was set at 20 in this paper, which is same as that in Ref. [34].

5.1.2. *Effect of mutation probability*

For simplicity, μ is denotes the linearly decreasing mutation probability used in this paper, which is formulated as $1-FES/Max\_FES$. Comparisons with other two constant mutation probabilities (0.5 and 1.0) were made to verify the effectiveness of μ. Fig. 7 illustrates the characteristics of three mutation probability strategies. The terminal criterion Max_FES was set as 150,000 for 30-Dim, 250,000 for 50-Dim, and 500,000 for 100-Dim respectively. Average simulation results over 50 runs are listed in Table 1, and the best results are highlighted in bold. It can be observed that μ achieved better results on eight of these nine cases than the other two constant values. Additionally, it significantly improved the results on multimodal function Shifted Rastrigin, which is more difficult to optimize than other two unimodal ones. All results demonstrate the effectiveness of the linearly decreasing strategy.

5.2. *Test on two decomposable problems with lower dimensions*

5.2.1. *Description of decomposable problems*

Real-valued decomposable problems are created by connecting basis functions, and the overall objective function values are equal to the sum of all the connected basis functions. Two types of real-valued decomposable problem are considered in this paper.

The first one is a real-valued deceptive problem (RDP) composed of trap functions [30], which are maximization problems. The mathematical formulation of the RDP problem is given below,

$$f_{RDP}(\mathbf{x}) = \sum_{i=1}^{m} f_{trap}(x_{2i-1}, x_{2i}) \tag{31}$$

where $x_k \in [0,1]$, $k \in \{1,2,\ldots,2m\}$, m denotes the number of subproblems, and the basis function f_{trap} is defined as below,

$$f_{trap}(x_{2i-1}, x_{2i}) = \begin{cases} \alpha, & \text{if } x_{2i-1}, x_{2i} \geq \delta \\ \frac{\beta}{\delta}\left(\delta - \sqrt{\frac{x_{2i-1}^2 + x_{2i}^2}{2}}\right), & \text{otherwise} \end{cases} \tag{32}$$

where α and β are the global and local optimum, respectively, and δ is the border of attractors.

The second problem is a real-valued nonlinear, symmetric problem (RNSP) that is composed of nonlinear, symmetric functions [30]. The RNSP problem is maximized as below,

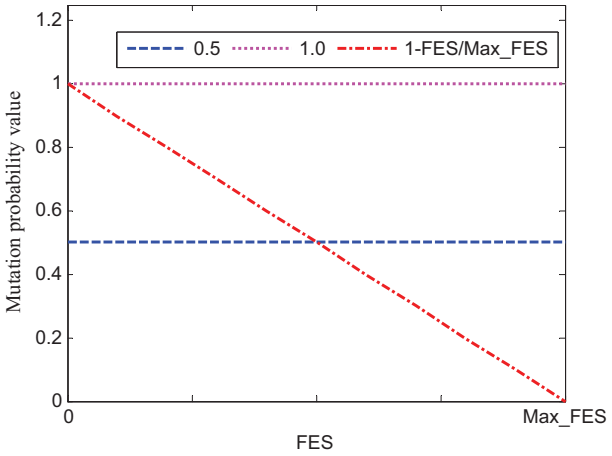

Fig. 7 – Three different mutation probabilities.

Table 1 – Comparison of average results among three different mutation strategies.

Function	Dim = 30			Dim = 50			Dim = 100		
	Mutation probability			Mutation probability			Mutation probability		
	0.5	1.0	μ	0.5	1.0	μ	0.5	1.0	μ
Shifted Sphere	5.30e-30	9.30e-30	**3.28e-30**	9.44e-29	**8.42e-29**	1.05e-28	1.76e-27	1.68e-27	**1.42e-27**
Shifted Rastrigin	2.02e + 01	1.13e + 02	**2.34e + 00**	4.90e + 01	2.68e + 02	**7.84e + 00**	2.35e + 02	6.96e + 02	**3.71e + 01**
Shifted Schwefel 1.2	3.48e-07	1.20e-06	**1.11e-07**	1.38e-02	3.61e-02	**7.45e-03**	8.74e + 01	1.88e + 02	**3.60e + 01**

The bold values signifies the best results obtained.

$$f_{RNSP}(\mathbf{x}) = \sum_{i=1}^{m} f_{nonsym}(x_{2i-1}, x_{2i}) \tag{33}$$

where $x_k \in [-5.12, 5.12]$, $k \in \{1, 2, \ldots, 2m\}$, m denotes the number of subproblems, and the basis nonlinear symmetric function f_{nonsym} is formulated as follows,

$$f_{nonsym}(x_{2i-1}, x_{2i}) = \begin{cases} 0.0, \text{ if } 1-\delta \le x_{2i-1}, x_{2i} \le 1+\delta \\ -100\left(x_{2i-1} - x_{2i}^2\right)^2 - (1-x_{2i})^2, \text{otherwise} \end{cases} \tag{34}$$

where δ adjusts the degree of building blocks supply.

Fig. 8 clearly illustrates the characteristics of two basis functions for RDP and RNSP.

5.2.2. *Parameter settings*

In the experiments, the parameter values for these two test problems are given as follows: RDP with $\alpha = 1.0$, $\beta = 0.8$, $\delta = 0.8$, and RNSP with $\delta = 0.2$. The STLBO was tested on these two problems with dimensions of 10, 20 and 30 (Dim = 2 m), and the Max_*FES* is set to 50,000, 100,000 and 150,000, respectively. All experiments were run 50 times independently.

Parameters of SaDE [35], GL-25 [36], IHS [37] and basic TLBO [34] are available in the references, and the remaining methods are set as below:

- ◇ STLBO - $ps = 20$;
- ◇ PSO-IW - $ps = 50$, $w_{start} = 0.9$, $w_{end} = 0.4$, $c_1 = c_2 = 2.0$ and $V_{max} = -V_{min} = 0.1 \times (UB - LB)$;
- ◇ PSO-CF - $ps = 50$, $\chi = 0.729$, $c_1 = c_2 = 2.05$ and $V_{max} = -V_{min} = 0.1 \times (UB - LB)$;
- ◇ GA-TB - $ps = 40$, $GGAP = 0.9$ and $PRECI = 20$,

where $GGAP$ denotes the generation gap, which determines how many new individuals are created; $PRECI$ is the precision of binary representation.

5.2.3. *Experimental results and discussions*

The global best of RDP is 5, 10, 15 for 10-Dim, 20-Dim and 30-Dim, respectively, and the best result of RNSP is 0 for all cases. Table 2 lists the best objective function values as well as the success rates by applying the eight methods to optimize the 10-Dim, 20-Dim and 30-Dim RDP and RNSP problems. In Table 2, *SR* denotes the rate of the method that reaches the global best within the specified Max_*FES* over 50 independent runs.

The proposed STLBO found the global optimum with 100% success rates on all RDP problems and two cases of RNSP problem, and the success rates for 30-Dim RNSP is 68%, which is competitive as well. Compared with other seven methods, STLBO exhibited better searching performance and scalability for different types and scales of problems. Although SaDE, GL-25 and IHS can also find the global best on two or three cases, their scalability is poor. For instance, GL-25 performed the best on all RNSP problems, while it never achieved the global best on RDP problems for all cases. The similar observations can also be found in SaDE and IHS. In comparison with the basic TLBO on these six cases, it is obvious that the performance of STLBO has been enhanced significantly.

5.3. *Test on large scale benchmark functions*

In this section, experiments were conducted on 12 shifted benchmark functions to investigate the performance of the proposed STLBO. Parameters for STLBO and for other seven methods in comparison are the same as those set in the above

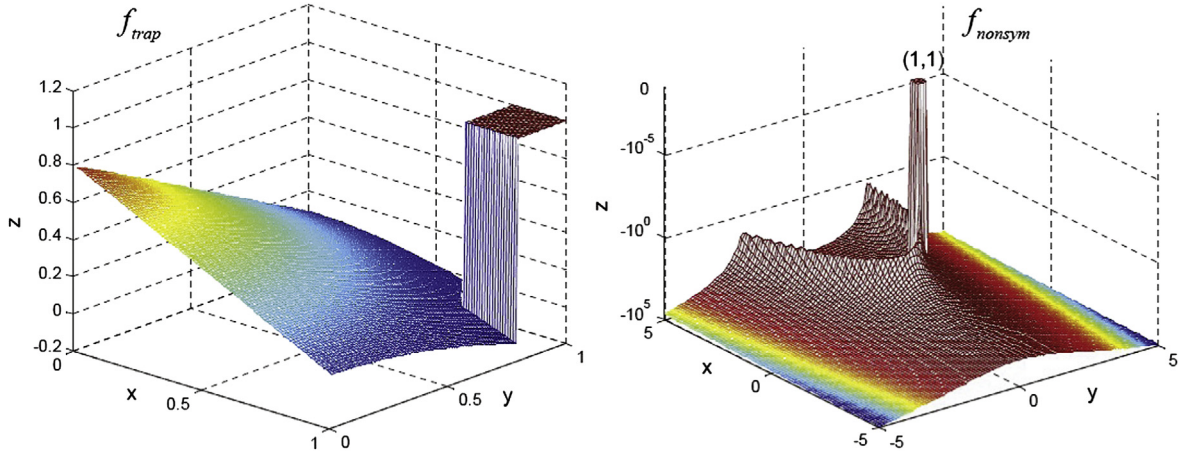

Fig. 8 – Basis functions of RDP and RNSP: f_{trap} and f_{nonsym}.

Table 2 – Comparison of best result and success rate on RDP and RNSP.

Method	Dim = 10				Dim = 20				Dim = 30			
	RDP		RNSP		RDP		RNSP		RDP		RNSP	
	Best	SR	Best	SR	Best	SR	Best	SR	Best	SR	Best	SR
SaDE	5	**100%**	0	**100%**	10	98%	0	10%	15	82%	−0.52	0%
GL-25	4.08	0%	0	**100%**	7.99	0%	0	**100%**	11.9	0%	0	**100%**
PSO-IW	5	10%	0	88%	9.23	0%	−0.33	0%	13.1	0%	−1.32	0%
PSO-CF	5	18%	0	**100%**	9.45	0%	0	60%	13.4	0%	−0.03	0%
IHS	5	**100%**	0	42%	10	**100%**	−0.49	0%	15	**100%**	−2.03	0%
GA-TB	5	26%	−0.31	0%	9.80	0%	−0.92	0%	14.4	0%	−2.41	0%
TLBO	5	8%	0	60%	9.19	0%	0	62%	13.4	0%	0	22%
STLBO	5	**100%**	0	**100%**	10	**100%**	0	**100%**	15	**100%**	0	68%

The bold values signifies the best success rates obtained.

section. The Max_*FES* was set to 500,000 for all these 100 dimensions problems and 50 independently runs were conducted for each function.

5.3.1. *Definition of benchmark functions*

Details of 12 commonly used benchmark functions are listed in Table 3. Dim denotes the dimension of the problem, Boundary denotes the searching space of the decision variables, Min$f(\cdot)$ is the global optimum.

Functions from f_1 to f_5 are all unimodal with their global best solutions locating at the center of the searching space, f_5 is a discontinuous one, f_6 is the multimodal Rosenbrock characterized by an extremely deep valley along the parabola that leads to the global optimum [31]. Functions from f_6 to f_{12} are multimodal, wherein the number of local optimum increases exponentially with the increase of problem dimensions. As many methods are specially developed for problems with global best solution located at the center of searching space, tests on basic benchmark functions are not enough for a thorough evaluation of the performance. To make a fair evaluation of the performance of different methods, the global best solution was shifted to a random position in its searching space, which is more consistent in practice [35]. The shift strategy has been applied to all the 12 problems, which cover different types of problems, including unimodal, discontinuous and multimodal. Compared with the conventional benchmark problems, the shifted ones are more challenging, and have been used in numerical optimization [35,40,41]. In Table 3, y is the decision variable after being shifted, which can be presented as $\mathbf{y} = \mathbf{x} - \mathbf{o}$. Vector $\mathbf{o}$ is the shifted distance that is generated randomly in the searching space,

$$o_k = \text{rand} \times [UB_k - LB_k] + LB_k, \quad k \in \{1, 2, \ldots, \text{Dim}\} \tag{35}$$

Once the shifted distance vector $\mathbf{o}$ is produced, it is kept constant and applied for all other problems in the same searching space.

Table 3 – Formulations of Benchmark functions.

No.	Function	Formulation	Type	Dim	Boundary	Min $f(\cdot)$
1	Shifted Sphere	$f_1(\mathbf{x}) = \sum_{i=1}^{\text{Dim}} y_i^2$	Unimodal	100	[−100,100]	0
2	Shifted Quatic	$f_2(\mathbf{x}) = \sum_{i=1}^{\text{Dim}} i y_i^4$	Unimodal	100	[−1.28,1.28]	0
3	Shifted Schwefel 2.21	$f_3(\mathbf{x}) = \max\{\lvert y_i \rvert, 1 \le i \le \text{Dim}\}$	Unimodal	100	[−100,100]	0
4	Shifted Schwefel 1.2	$f_4(\mathbf{x}) = \sum_{i=1}^{\text{Dim}} (\sum_{j=1}^{i} y_j)^2$	Unimodal	100	[−100,100]	0
5	Shifted Step	$f_5(\mathbf{x}) = \sum_{i=1}^{\text{Dim}} (\lfloor y_i + 0.5 \rfloor)^2$	Discontinuous	100	[−100,100]	0
6	Shifted Rosenbrock	$f_6(\mathbf{x}) = \sum_{i=1}^{\text{Dim}-1} \{100 \cdot (y_{i+1} - y_i)^2 + (1 - y_i)^2\}$	Multimodal	100	[−30,30]	0
7	Shifted Rastrigin	$f_7(\mathbf{x}) = \sum_{i=1}^{\text{Dim}} \{y_i^2 - 10\cos(2\pi y_i) + 10\}$	Multimodal	100	[−5.12,5.12]	0
8	Shifted Griewank	$f_8(x) = \sum_{i=1}^{\text{Dim}} \frac{y_i^2}{4000} - \prod_{i=1}^{\text{Dim}} \cos\left(\frac{y_i}{\sqrt{i}}\right) + 1$	Multimodal	100	[−600,600]	0
9	Shifted Ackley	$f_9(x) = -20\exp\left(-0.2\sqrt{\frac{1}{\text{Dim}}\sum_{i=1}^{\text{Dim}} y_i^2}\right) - \exp\left(\frac{1}{\text{Dim}}\sum_{i=1}^{\text{Dim}} \cos(2\pi y_i)\right) + 20 + e$	Multimodal	100	[−32,32]	0
10	Shifted Salmon	$f_{10}(\mathbf{x}) = 1 - \cos\left(2\pi\sqrt{\sum_{i=1}^{\text{Dim}} y_i^2}\right) + 0.1\sqrt{\sum_{i=1}^{\text{Dim}} y_i^2}$	Multimodal	100	[−100,100]	0
11	Shifted Penalized	$f_{11}(\mathbf{x}) = 0.1 \cdot \sin^2(3\pi y_1) + \sum_{i=1}^{\text{Dim}} u(y_i, 5, 100, 4) + 0.1 \cdot \sum_{i=1}^{\text{Dim}-1} (y_i - 1)^2 [1 + \sin^2(3\pi y_{i+1})] + 0.1 \cdot (y_{\text{Dim}} - 1)^2 [1 + \sin^2(2\pi y_{\text{Dim}})]$ $u(y_i, a, k, m) = \begin{cases} k(y_i - a)^m, & y_i > a \\ 0, & -a \le y_i \le a \\ k(-y_i - a), & y_i < -a \end{cases}$	Multimodal	100	[−50,50]	0
12	Shifted Levy	$f_{12}(\mathbf{x}) = \sum_{i=1}^{\text{Dim}-1} (y_i - 1)^2 \times (1 + \sin^2(3\pi y_{i+1})) + (y_{\text{Dim}} - 1)^2 (1 + \sin^2(2\pi y_{\text{Dim}})) + \sin^2(3\pi y_1)$	Multimodal	100	[−10,10]	0

Table 4 – Comparison of eight methods on average results over 50 runs for 100D.

No.	Function		Method							
			SaDE	GL-25	PSO-IW	PSO-CF	IHS	GA-Tb	TLBO	STLBO
f_1	Shifted Sphere	Ave	**4.46e-28**	2.23e-09	1.36e + 02	7.97e + 02	7.40e + 03	3.27e-07	4.50e-26	1.64e-27
		Std	**5.22e-28**	1.57e-08	1.03e + 02	6.14e + 02	7.63e + 02	3.20e-22	2.06e-25	1.46e-27
f_2	Shifted Quatic	Ave	6.23e-38	3.69e-21	1.13e-01	3.39e-01	3.56e + 00	2.73e-21	7.45e-28	**1.13e-52**
		Std	1.36e-37	2.61e-20	1.03e-01	2.05e-01	8.76e-01	1.90e-36	5.26e-27	**4.79e-52**
f_3	Shifted Schwefel 2.21	Ave	3.57e + 01	4.19e + 01	1.29e + 01	1.28e + 01	3.63e + 01	**9.62e + 00**	7.90e + 01	3.13e + 01
		Std	7.06e + 00	3.65e + 00	**8.95e-01**	1.26e + 00	1.94e + 00	1.99e + 00	4.52e + 00	3.95e + 00
f_4	Shifted Schwefel 1.2	Ave	1.93e + 03	2.40e + 04	1.68e + 04	2.53e + 04	1.49e + 05	3.71e + 04	1.10e + 04	**5.52e + 01**
		Std	6.73e + 02	7.70e + 03	5.97e + 03	2.41e + 04	2.27e + 04	6.69e + 03	6.94e + 03	**2.08e + 01**
f_5	Shifted Step	Ave	**0**	1.66e + 02	1.62e + 02	1.33e + 03	7.54e + 03	2.18e + 02	5.72e + 02	3.86e + 00
		Std	**0**	5.90e + 01	1.15e + 02	8.54e + 02	9.87e + 02	3.94e + 02	8.51e + 02	2.00e + 00
f_6	Shifted Rosenbrock	Ave	2.01e + 02	3.01e + 02	2.90e + 04	7.90e + 04	2.61e + 06	3.27e + 02	1.72e + 02	**1.18e + 02**
		Std	5.20e + 01	1.12e + 02	2.59e+04	7.52e + 04	5.19e + 05	2.20e + 02	5.03e + 01	**3.76e + 01**
f_7	Shifted Rastrigin	Ave	1.22e + 02	1.89e + 02	4.53e + 02	7.06e + 02	2.08e + 02	1.94e + 02	4.74e + 02	**3.59e + 01**
		Std	1.59e + 01	2.78e + 01	7.47e + 01	6.54e + 01	1.67e + 01	3.11e + 01	5.13e + 01	**7.54e + 00**
f_8	Shifted Griwank	Ave	2.03e-02	8.76e-02	5.21e + 00	1.95e + 01	7.07e + 01	1.32e-01	6.17e-02	**6.20e-03**
		Std	4.44e-02	9.57e-02	2.42e + 00	8.78e + 00	8.85e + 00	2.40e-01	1.99e-01	**8.24e-03**
f_9	Shifted Ackley	Ave	3.05e + 00	2.91e + 00	**5.13e-01**	1.88e + 01	1.01e + 01	2.31e + 00	6.88e + 00	8.53e-01
		Std	7.90e-01	**3.92e-01**	2.81e + 00	1.95e + 00	3.97e-01	1.37e + 00	2.08e + 00	1.62e + 00
f_{10}	Shifted Salmon	Ave	**1.32e + 00**	1.54e + 00	2.38e + 00	4.40e + 00	1.13e + 01	8.08e + 00	1.74e + 00	1.74e + 00
		Std	4.79e-01	4.00e-01	6.13e-01	9.84e-01	8.34e-01	1.19e + 00	5.98e-01	**2.85e-01**
f_{11}	Shifted Penalized	Ave	5.15e + 00	4.35e + 00	5.21e-02	1.41e + 01	1.20e + 06	4.50e-02	1.26e + 02	**9.99e-03**
		Std	1.49e + 01	6.95e + 00	1.74e-01	1.51e + 01	3.59e + 05	1.72e-01	1.36e + 02	**1.48e-02**
f_{12}	Shifted Levy	Ave	2.88e-01	1.33e-01	1.34e + 01	2.58e + 02	1.19e + 02	1.64e + 00	1.61e + 00	**8.31e-02**
		Std	8.22e-01	1.89e-01	5.62e + 00	1.86e + 02	1.59e + 01	4.75e + 00	4.47e + 00	**8.93e-02**

The bold values signifies the best results obtained.

5.3.2. *Experimental results and discussions*

Mean results of the 50 runs of the eight algorithms on the 12 test problems with 100 dimensions are summarized in Table 4, wherein the best results are shown in bold. In Table 4, 'Ave' is the average result among 50 runs, and 'Std' is the standard deviation.

For the unimodal problems, STLBO achieved better results on f_2 (Shifted Quatic) and f_4 (Shifted Schwefel 1.2) with significant improvements. STLBO performed slightly worse than SaDE and GA-TB on f_1 (Shifted Sphere) and f_3 (Shifted Schwefel 2.21) respectively, but it is still competitive when compared with other six methods. Furthermore, STLBO outperformed all the other methods on five of the seven multimodal problems, which indicates its ability in solving complicated problems. Meanwhile, it also ranks the second and the third on f_9 (Shifted Ackley) and f_{10} (Shifted Salmon), respectively. As a whole, the STLBO achieves much better performance than other methods in terms of solution accuracy. Compared with the basic TLBO, the STLBO achieves better results on almost all problems, and performs particular well on f_2, f_4, f_{11} and f_{12}. Moreover, it can also be found that the STLBO is the most stable one for its smaller Std values on these examples.

In order to illustrate the computational results, box-plots are used to show the distribution of results obtained by each algorithm over 50 runs. These box-plots are shown in Fig. 9.

Compared with the basic TLBO, the improvement by the proposed STLBO is obvious. Compared with the most competitive reference algorithm (SaDE), the STLBO also exhibits significant advantages in the solutions quality and robustness, which is shown from the span of the solution distributions.

6. Application to the parameter identification of PEM fuel cell and solar cell models

To evaluate the identification ability of the STLBO on parameter estimation problems, it is used to extract the parameters in the PEM fuel cell model in Ref. [1] as well as the solar cell model in Ref. [13].

6.1. *Parameter estimation of PEM fuel cell model*

In this section, the basic TLBO [34], SaDE [35], GL-25 [36], IHS [37], PSO-CF [38], and the proposed STLBO were employed to optimize the PEM fuel cell model parameters. To make a fair comparison, the Max_*FES* was set to 20,000, and other parameters remained unchanged.

Operational parameters of the PEM fuel cells were taken from Ref. [1] and are listed in Table 5. The experimental data used for parameter identification was taken from Ref. [2]. Two sets of experimental data (3/5 bar, 353.15 K), (1/1 bar, 343.15 K) were utilized to estimate the seven model parameter and other two sets of data (2.5/3 bar, 343.15 K) and (1.5/1.5 bar, 343.15 K) were used for validation. Thus, values of *S* and *N* in Eq. (14) are 2 and 15, respectively. Additionally, the ranges of parameters play an important effect on the estimation performance [2], and relative wider ranges could result in a better fit. Therefore, three different searching ranges taken from Refs. [1,2,5] were considered in this paper, and listed in Table 6. The identification results and validation results with three different ranges are illustrated in Fig. 10. It is shown that the estimated voltages match well with the

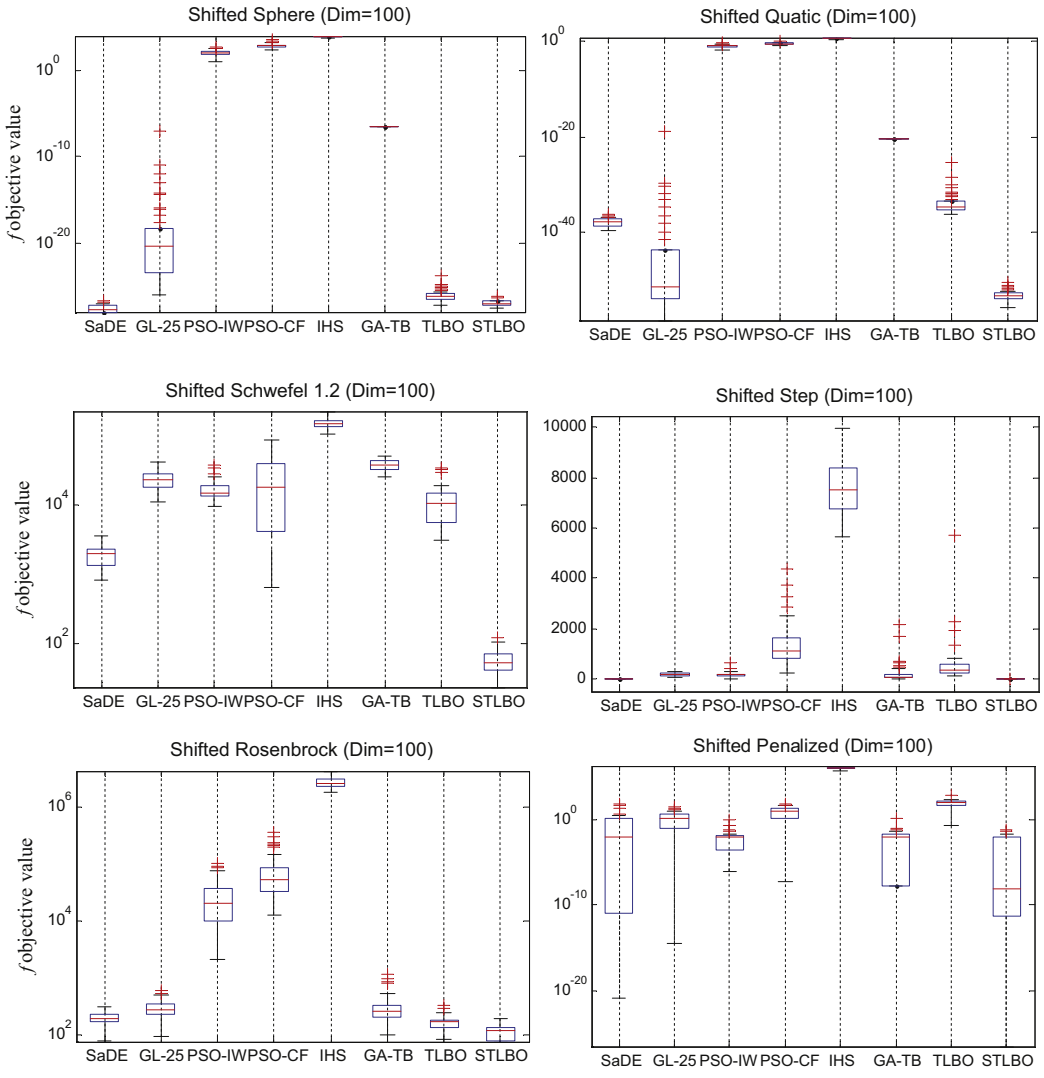

Fig. 9 – Boxplot of best objective values over 50 runs on f_1, f_2, f_3, f_5, f_6 and f_{11}.

experimental data. Moreover, it can also be found that a wider searching range contributes to improved accuracy of the identified solutions.

To assess how well the model with the estimated parameters matches the original system, the 'Error', which is the sum of SSE for all four data sets, were compared for different methods. Once the model parameters were identified based on data sets 1 and 2, they were used to calculate the 'Error'. Comparisons with other methods in terms of sum of SSE for all the four data sets are listed in Table 7. It is clear that the smaller the 'Error' value, the better the identified parameters. According to Table 7, the STLBO performed as equally well (the best) as the TLBO and GL-25 on Range 1, while it further yielded the smallest 'Error' value on Ranges 2 and 3. As a whole, in this study, the STLBO has produced the best results on PEM fuel cell problems with different ranges. Further, it is also shown that the basic TLBO and SaDE are competitive compared with other methods.

6.2. *Parameter estimation of solar cell model*

In this section, the measured $I - U$ data taken from Refs. [13,42], which was acquired from a commercial silicon solar cell system (1000 W/m^2) at 33 °C, was used to evaluated the efficiency of the proposed STLBO. The searching range of the solar cell parameters are shown in Table 8, and Table 9 shows

Table 5 – Operational parameters of a 250 W PEM fuel cell model.

Parameters	Value	Parameters	Value
n	24	RH_a	1
A (cm^2)	27	RH_c	1
l (μm)	127	P_a (bar)	1.0–3.0
J_{max} (A/cm^2)	0.86	P_c (bar)	1.0–5.0
Power (W)	250	T (K)	343.15–353.15

Table 6 – Three different searching ranges of model parameters.

Model parameters	ξ_1	ξ_2	ξ_3	ξ_4	λ	R_C (Ω)	b (V)
Lower range 1 [1]	−9.52e-01	1.00e-03	7.40e-05	−1.98e-04	14	1.00e-04	1.60e-02
Upper range 1 [1]	−9.44e-01	5.00e-03	7.80e-05	−1.88e-04	23	8.00e-04	5.00e-01
Lower range 2 [2]	−1.19969	1.00e-03	3.60e-05	−2.60e-04	10	1.00e-04	1.36e-02
Upper range 2 [2]	−0.8532	5.00e-03	9.80e-05	−9.54e-05	24	8.00e-04	5.00e-01
Lower range 3 [5]	−1.20	8.00e-04	3.50e-05	−3.00e-04	10	8.00e-05	1.00e-02
Upper range 3 [5]	−0.80	6.00e-03	1.00e-04	−8.00e-05	24	9.90e-04	6.00e-01

the measured $I-U$ data. 30 independent runs were carried out on double and single diode models with Max_*FES* of 50,000.

The objective function Y defined in (18) needs to be minimized in order to find the optimal set of parameters that accurately reflect the solar cell characteristics. Table 10 summarizes the identified parameters and corresponding objective values for the double diode model. The results obtained by STLBO are compared with the basic TLBO and other four reported results in literature, including results obtained by ABSO [13], IGHS [43], pattern search (PS) [12] and simulated annealing (SA) [11]. From the Y values, it is evident that the proposed STLBO outperformed all the other five methods with the minimal objective value of **9.8248e-04**, which indicates that the parameters identified by STLBO is the closest to the real system parameters. To make a further investigation on the quality of the parameters obtained by STLBO, these parameters were put into the double diode model to reconstruct the $I-U$ and $P-U$ characteristics. Fig. 11 illustrates these two

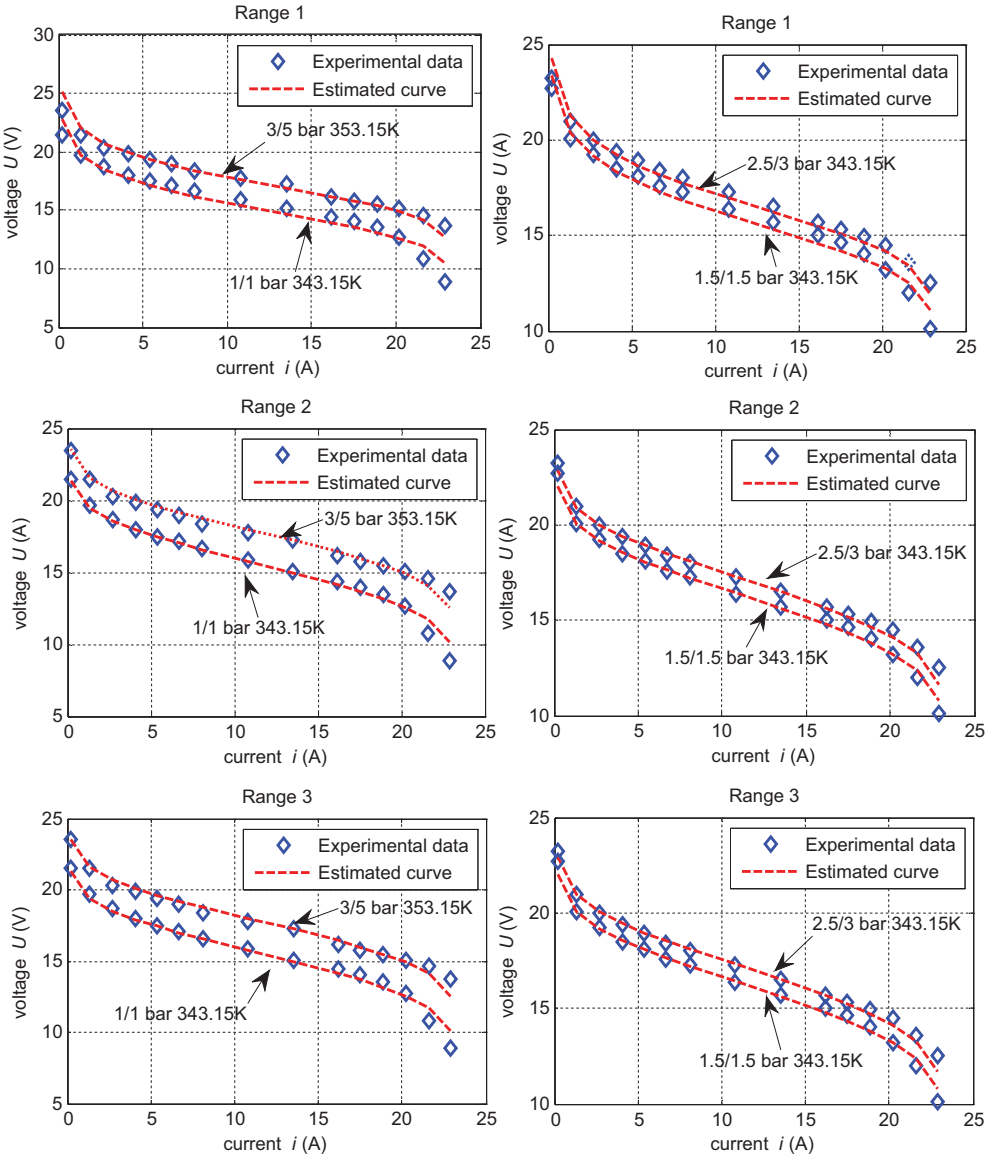

Fig. 10 – PEM fuel cell stack experimental data and estimated curve obtained by STLBO – Left sides are identification results and right sides are validation results.

Table 7 – Comparison with other methods on the sum of SSE for all four data sets.

Methods	Error	Parameters						
		ξ_1	ξ_2	ξ_3	ξ_4	λ	R_C (Ω)	b (V)
Range 1								
Real GA [2]	16.2746	−0.9506	3.0842e-03	7.7524e-05	−1.8803e-04	22.9906	1.0027e-04	0.0329
SaDE	16.2369	−0.9520	2.9400e-03	7.8000e-05	−1.8800e-04	23	1.0000e-04	3.2812e-02
PSO-CF	16.2846	−0.9481	2.9285e-03	7.8000e-05	−1.8800e-04	22.8374	1.0000e-04	3.2510e-02
GL-25	**16.2363**	−0.9520	2.9400e-03	7.8000e-05	−1.8800e-04	23	1.0000e-04	3.2813e-02
IHS	16.2372	−0.9520	2.9400e-03	7.8000e-05	−1.8800e-04	23	1.0000e-04	3.2815e-02
TLBO	**16.2363**	−0.9520	2.9400e-03	7.8000e-05	−1.8800e-04	23	1.0000e-04	3.2813e-02
STLBO	**16.2363**	−0.9520	2.9400e-03	7.8000e-05	−1.8800e-04	23	1.0000e-04	3.2813e-02
Range 2								
Real GA [2]	8.4854	−1.1568	3.4243e-03	6.4161e-05	−1.1544e-04	12.8989	1.4504e-04	0.0343
SaDE	7.6276	−0.8534	2.5846e-03	7.5880e-05	−1.1540e-04	12.6051	1.0000e-04	3.2973e-02
PSO-CF	7.7180	−0.8889	2.6656e-03	7.5314e-05	−1.1543e-04	12.6130	1.0000e-04	3.2992e-02
GL-25	7.9559	−0.9655	2.8392e-03	7.1857e-05	−1.1543e-04	12.6097	1.0000e-04	3.2980e-02
IHS	8.4672	−1.0820	3.0921e-03	6.5776e-05	−1.1491e-04	12.5254	1.0000e-04	3.2780e-02
TLBO	7.6426	−0.8532	2.5856e-03	7.6997e-05	−1.1529e-04	12.5848	1.0000e-04	3.2940e-02
STLBO	**7.6266**	−0.8532	2.5843e-03	7.6892e-05	−1.1541e-04	12.6079	1.0000e-04	3.2978e-02
Range 3								
SaDE	7.5086	−0.8012	2.4661e-03	7.9206e-05	−1.1546e-04	12.5734	8.0003e-05	3.2956e-02
PSO-CF	7.7594	−0.9031	2.6969e-03	7.4605e-05	−1.1544e-04	12.5710	8.0000e-05	3.2949e-02
GL-25	7.8803	−0.9428	2.7873e-03	7.2835e-05	−1.1546e-04	12.5731	8.0000e-05	3.2957e-02
IHS	8.7506	−1.1402	3.2397e-03	6.4277e-05	−1.1464e-04	12.2716	8.0000e-05	3.1932e-02
TLBO	7.5500	−0.8196	2.5087e-03	7.8437e-05	−1.1542e-04	12.5684	8.0000e-05	3.3029e-02
STLBO	**7.5069**	−0.8000	2.4632e-03	7.9252e-05	−1.1545e-04	12.5719	8.0000e-05	3.2952e-02

The bold values signifies the best results obtained.

type of characteristics derived from the measured data and the estimated double diode model. It is obvious that the estimated curve is in good agreement with the measured data, which indicates the accuracy of the estimated parameters.

Simulation results on the single diode model are shown in Table 11 along with comparable results reported from previous studies. The objective value Y obtained using STLBO is **9.8602e-04**, which is better than all the other reported outcomes and that of the basic TLBO. Further, compared with the double diode model, Y is slightly bigger for the single diode model, which clearly indicates that the double diode model is slightly more accurate than the single diode one. Fig. 12 illustrates the $I-U$ and $P-U$ characteristics derived from the measured data and single diode model. It reveals that the estimated curve is in good agreement with the experimental data.

Table 8 – Upper and lower range of solar cell parameters [13].

Parameters	R_s (Ω)	R_{sh} (Ω)	I_{ph} (A)	I_{sd} (μA)	n
Lower	0	0	0	0	1
Upper	0.5	100	1	1	2

In order to demonstrate the efficiency of the proposed STLBO for the solar cell problem, the distributions of the best results of each independent run are illustrated in Fig. 13. It is obvious that all results obtained by STLBO are lower than the basic TLBO. Compared with basic TLBO, the results obtained by STLBO have smaller variations for different runs, which indicates the robustness of the proposed method for the solar cell problems. From the simulation results of two solar cell models, it confirms that the proposed STLBO always produces better quality solutions than the basic TLBO, and is also more robust.

7. Conclusion

In this paper, an improved and simplified TLBO with elite strategy (STLBO) has been proposed to identify the unknown parameters in the complex nonlinear PEM fuel cell and solar cell models. This new algorithm has the advantages of being easy to understand and simple to implement and thus can be easily used to solve a wide range of design and optimization problems. The STLBO is able to increase the probability of searching better solutions while the diversity of the

Table 9 – Measured data for double and single diode models.

No.	1	2	3	4	5	6	7	8	9	10	11	12	13
U (V)	−0.2057	−0.1291	−0.0588	0.0057	0.0646	0.1185	0.1678	0.2132	0.2545	0.2924	0.3269	0.3585	0.3873
I (A)	0.764	0.762	0.7605	0.7605	0.76	0.759	0.757	0.757	0.7555	0.754	0.7505	0.7465	0.7385
No.	14	15	16	17	18	19	20	21	22	23	24	25	26
U (V)	0.4137	0.4373	0.459	0.4784	0.496	0.5119	0.5265	0.5398	0.5521	0.5633	0.5736	0.5833	0.59
I (A)	0.728	0.7065	0.6755	0.632	0.573	0.499	0.413	0.3165	0.212	0.1035	−0.01	−0.123	−0.21

Table 10 – Comparison of best results on the double diode model.

Method	Y	Parameters						
		R_s (Ω)	R_{sh} (Ω)	I_{ph} (A)	I_{sd1} (μA)	I_{sd2} (μA)	n_1	n_2
PS [12]	0.01518	0.0320	81.3008	0.7602	0.9889	0.0001	1.6000	1.1920
SA [11]	0.01664	0.0345	43.1034	0.7623	0.4767	0.0100	1.5172	2.0000
IGHS [43]	9.8635e-04	0.03690	56.8368	0.76079	0.97310	0.16791	1.92126	1.42814
ABSO [13]	9.8344e-04	0.03657	54.6219	0.76078	0.26713	0.38191	1.46512	1.98152
TLBO	9.9507e-04	0.03646	55.8459	0.76067	0.20289	0.29948	1.99809	1.47494
STLBO	**9.8248e-04**	0.03674	55.4920	0.76078	0.22566	0.75217	1.45085	2.00000

The bold values signifies the best results obtained.

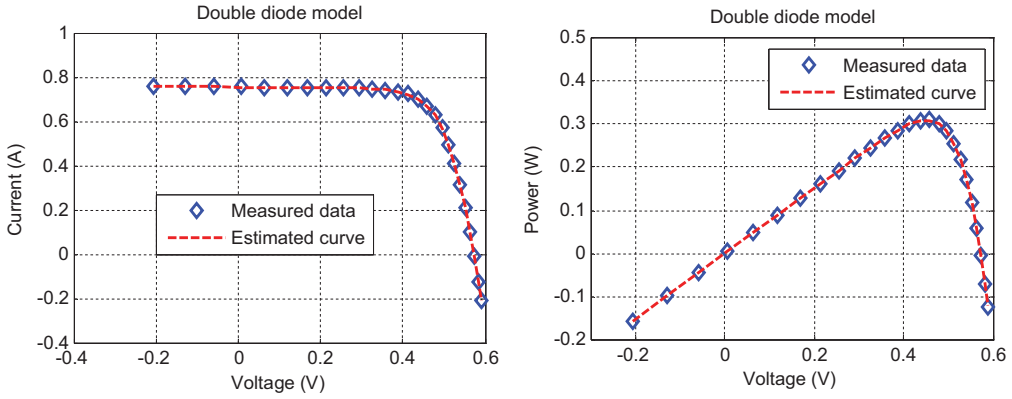

Fig. 11 – Comparison between the $I - U/P - U$ characteristics obtained from the measured data and the double diode model.

Table 11 – Comparison of best results on the single diode model.

Parameter	Method							
	CPSO [10]	PS [12]	SA [11]	GGHS [43]	ABSO [13]	IADE [14]	TLBO	STLBO
R_s (Ω)	0.0354	0.0313	0.0345	0.03631	0.03659	0.03621	0.03641	0.03638
R_{sh} (Ω)	59.012	64.1026	43.1034	53.0647	52.2903	54.7643	54.4029	53.7187
I_{ph} (A)	0.7607	0.7617	0.7620	0.76092	0.76080	0.7607	0.76074	0.76078
I_{sd} (μA)	0.4000	0.9980	0.4798	0.32620	0.30623	0.33613	0.32378	0.32302
n	1.5033	1.6000	1.5172	1.48217	1.47583	1.4852	1.48136	1.48114
Y	0.00139	0.01494	0.01900	9.9097e-04	9.9124e-04	9.8900e-04	9.8845e-04	**9.8602e-04**

The bold values signifies the best results obtained.

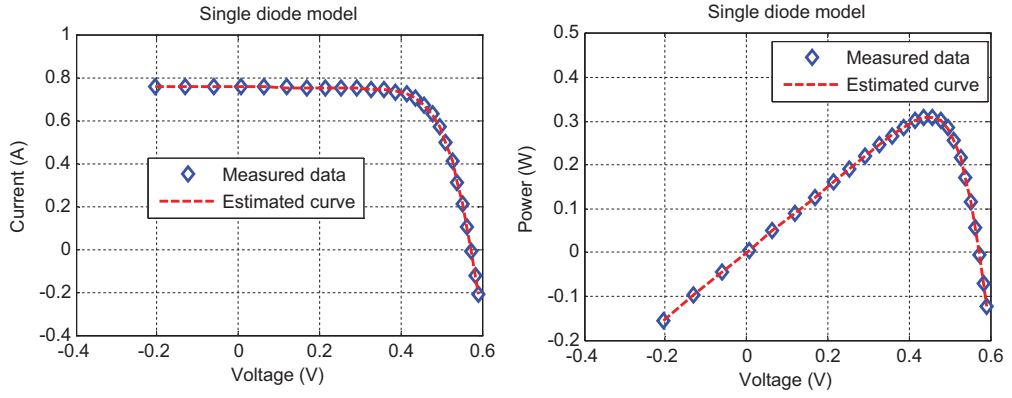

Fig. 12 – Comparison between the $I - U/P - U$ characteristics obtained from the measured data and the single diode model.

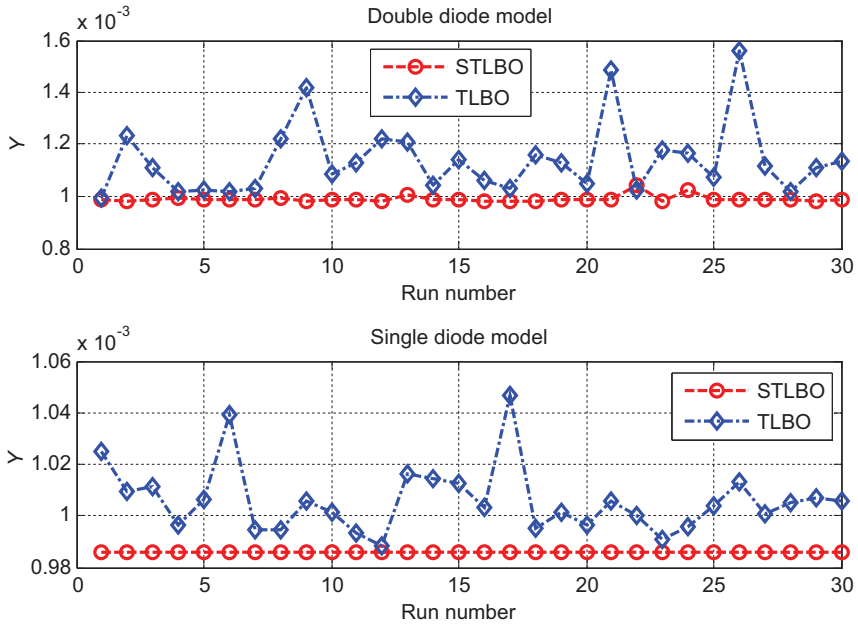

Fig. 13 – Distribution of best results over 30 independent runs.

populations are maintained by using elite strategy and linearly decreasing mutation probability. Simulation results on a group of benchmark problems reveal that the STLBO can find better solutions than the basic TLBO and other six commonly used methods. Further, the proposed method is applied to two real world parameter identification problems for PEM fuel cell and solar cell models, and experimental results demonstrate that the STLBO can produce the best results for PEM fuel cell models with three different searching ranges and solar cell models with double diode and single diode. It is also shown that the STLBO performs more effectively in comparison with reported results and the basic TLBO algorithm. Hence, we believe STLBO is a promising and effective method for parameter identification of PEM fuel cell and solar cell models, and it is also a promising alternative for other complex real world optimization problems.

Acknowledgments

This work is supported by the National Natural Science Foundation of China (61273040), Shanghai Rising-Star Program (12QA1401100), and the Project of Shanghai Municipal Education Commission (12YZ020).

REFERENCES

[1] Mo ZJ, Zhu XJ, Wei LY, Cao GY. Parameter optimization for a PEMFC model with a hybrid genetic algorithm. Int J Energy Res 2006;30(8):585–97.
[2] Ohenoja M, Leiviska K. Validation of genetic algorithm results in a fuel cell model. Int J Hydrogen Energy 2010;35(22):12618–25.
[3] Zhang L, Wang N. An adaptive RNA genetic algorithm for modeling of proton exchange membrane fuel cells. Int J Hydrogen Energy 2013;38(1):219–28.
[4] Chakraborty UK, Abbott TE, Das SK. PEM fuel cell modeling using differential evolution. Energy 2012;40(1):387–99.
[5] Yang SP, Wang N. A novel P system based optimization algorithm for parameter estimation of proton exchange membrane fuel cell model. Int J Hydrogen Energy 2012;37(10):8465–76.
[6] Ye MY, Wang XD, Xu YS. Parameter identification for proton exchange membrane fuel cell model using particle swarm optimization. Int J Hydrogen Energy 2009;34(2):981–9.
[7] Askarzadeh A, Rezazadeh A. A grouping-based global harmony search algorithm for modeling of proton exchange membrane fuel cell. Int J Hydrogen Energy 2011;36(8):5047–53.
[8] Askarzadeh A, Rezazadeh A. An innovative global harmony search algorithm for parameter identification of a PEM fuel cell model. IEEE Trans Ind Electron 2012;59(9):3473–80.
[9] Askarzadeh A, Rezazadeh A. A new heuristic optimization algorithm for modeling of proton exchange membrane fuel cell: bird mating optimizer. Int J Energy Res 2013;37(10):1196–204.
[10] Huang W, Jiang C, Xue LY, Song DY. Extracting solar cell model parameters based on chaos particle swarm algorithm. In: IEEE world congress on electric information and control engineering (ICEICE 2011) 2011. pp. 398–402.
[11] EI-Naggar KM, AIRashidi MR, AIHajri MF, AI-Othman AK. Simulated annealing algorithm for photovoltaic parameters identification. Sol Energy 2012;86(1):266–74.
[12] AIHajri MF, EI-Naggar KM, AIRashidi MR, AI-Othman AK. Optimal extraction of solar cell parameters using pattern search. Renew Energy 2012;44:238–45.
[13] Askarzadeh A, Rezazadeh A. Artificial bee swarm optimization algorithm for parameters identification of solar cell models. Appl Energy 2013;102:943–9.
[14] Jiang LL, Maskell DL, Patra JC. Parameter estimation of solar cells and modules using an improved adaptive differential evolution algorithm. Appl Energy 2013;112:185–93.

[15] Askarzadeh A. Parameter estimation of fuel cell polarization curve using BMO algorithm. Int J Hydrogen Energy 2013;38(35):15405–13.
[16] Rao RV, Savsani VJ, Vakharia DP. Teaching-learning-based optimization: a novel method for constrained mechanical design optimization problems. CAD Comput Aided Des 2011;43(3):303–15.
[17] Rao RV, Patel V. An elitist teaching-learning-based optimization algorithm for solving complex constrained optimization problems. Int J Ind Eng Comput 2012;3(4):535–60.
[18] Rao RV, Patel V. Comparative performance of an elitist teaching-learning-based optimization algorithm for solving unconstrained optimization problems. Int J Ind Eng Comput 2013;4(1):29–50.
[19] Crepinsek M, Liu SH, Mernik L. A note on teaching-learning-based optimization algorithm. Inf Sci 2012;212:79–93.
[20] Amphlett JC, Baumert RM, Mann RF, Peppley BA, Roberge PR. Performance modeling of the ballard mark IV solid polymer electrolyte fuel cell. J Electrochem Soc 1995;142(1):1–15.
[21] Correa JM, Faret FA, Popov VA, Simoes MG. Sensitivity analysis of the modeling parameters used in simulation of proton exchange membrane fuel cells. IEEE T Energ Conver 2005;20(1):211–8.
[22] Mann RF, Amphlett JC, Hooper MAI, Jensen HM, Peppley BA, Roberge PR. Development and application of a generalized steady-state electrochemical model for a PEM fuel cell. J Power Sources 2000;86(1):173–80.
[23] Nguyen TV, White RE. A water and heat management model for proton-exchange-membrane fuel cells. J Electrochem Soc 1993;140(8):2178–86.
[24] Wolf M, Noel GT, Stirm RJ. Investigation of the double exponential in the current-voltage characteristics of silicon solar cells. IEEE Trans Electron Devices 1977;ED-24(4):419–28.
[25] Rao RV, Patel V. Multi-objective optimization of heat exchanger using a modified teaching-learning-based optimization algorithm. Appl Math Model 2011;37(3):1147–62.
[26] Niknam T, Azizipanah-Abarghooee R, Aghaei J. A new modified teaching-learning algorithm for reserve constrained dynamic economic dispatch. IEEE Trans Power Syst 2013;28(2):749–63.
[27] Martin-Mena AJ, Gil-Mena JA. Optimal distributed generation location and size using a modified teaching-learning based optimization algorithm. Int J Electr Power Energy Syst 2013;50(1):65–75.
[28] Rao RV, Kalyankar VD. Parameter optimization of modern machining process using teaching-learning-based optimization algorithm. Eng Appl Artif Intell 2013;26(1):524–31.
[29] May RM. Simple mathematical models with very complicated dynamics. Nature 1976;261:459–67.
[30] Ahn CW, Ramakrishna RS. On the scalability of real-coded bayesian optimization algorithm. IEEE Trans Evol Comput 2008;12(3):307–22.
[31] Yao X, Liu Y, Lin GM. Evolutionary programming made faster. IEEE Trans Evol Comput 1999;3(2):82–102.
[32] Rahnamayan S, Tizhoosh HR, Salama MMA. Opposition-based differential evolution. IEEE Trans Evol Comput 2008;12(1):64–79.
[33] Montes Do Oca MA, Stutzle T, Van Den Enden K, Dorigo M. Incremental social learning in particle swarms. IEEE Trans Syst Man Cybern Part B Cybern 2011;41(2):368–84.
[34] Rao RV, Savsani VJ, Vakharia DP. Teaching-learning-based optimization: an optimization method for continuous non-linear large scale problems. Inf Sci 2012;183(1):1–15.
[35] Qin AK, Huang VL, Suganthan PN. Differential evolution algorithm with strategy adaptation for global numerical optimization. IEEE Trans Evol Comput 2009;13(2):398–417.
[36] Garcia-Martinez C, Lozano M, Herrera F, Molina D, Sanchez AM. Global and local real-coded genetic algorithms based on parent-centric crossover operators. Eur J Oper Res 2008;185(3):1088–113.
[37] Mahdavi M, Fesanghary M, Damangir E. An improved harmony search algorithm for solving optimization problems. Appl Math Comput J 2007;188(2):1567–79.
[38] Clerc M, Kennedy J. The particle swarm-explosion, stability, and convergence in a multidimensional complex space. IEEE Trans Evol Comput 2002;6(1):58–73.
[39] Shi YH, Eberhart R. A modified particle swarm optimizer. In: Proceeding of IEEE International Conference on Evolutionary Computation (ICEC 98) Anchorage 1998. pp. 69–73.
[40] Noman N, Iba H. Accelerating differential evolution using an adaptive local search. IEEE Trans Evol Comput 2008;12(1):107–25.
[41] Das S, Mukhopadhyay A, Roy A, Abraham A, Panigrahi B. Exploratory power of the harmony search algorithm: analysis and improvements for global numerical optimization. IEEE Trans Syst Man Cybern Part B Cybern 2011;41(1):89–106.
[42] Easwarakhanthan T, Bottin J, Bouhouch I. Nonlinear minimization algorithm for determining the solar cell parameters with microcomputers. Sol Energy 1986;4(1):4–12.
[43] Askarzadeh A, Rezazadeh A. Parameter identification for solar cell models using harmony search-based algorithms. Sol Energy 2012;86(11):3241–9.